ISSN 0021-3640, JETP Letters, 2022, Vol. 115, No. 9, pp. 495–501. © The Author(s), 2022. This article is an open access publication, corrected publication 2022.
ISSN 0021-3640, JETP Letters, 2022. © Pleiades Publishing, Inc., 2022.
Russian Text © The Author(s), 2022, published in Pis'ma v Zhurnal Eksperimental'noi i Teoreticheskoi Fiziki, 2022, Vol. 115, No. 9, pp. 547–553.

FIELDS, PARTICLES, AND NUCLEI

One-Loop Electroweak Radiative Corrections to Polarized Møller Scattering

S. G. Bondarenko[a, *], L. V. Kalinovskaya[b], L. A. Rumyantsev[b], and V. L. Yermolchyk[b, c]

[a] *Bogoliubov Laboratory of Theoretical Physics, Joint Institute for Nuclear Research, Dubna, Moscow region, 141980 Russia*

[b] *Dzhelepov Laboratory of Nuclear Problems, Joint Institute for Nuclear Research, Dubna, Moscow region, 141980 Russia*

[c] *Institute for Nuclear Problems, Belarusian State University, Minsk, 220006 Belarus*

**e-mail: bondarenko@jinr.ru*

Received March 20, 2022; revised March 27, 2022; accepted March 27, 2022

This work is devoted to a theoretical description of polarized Møller scattering. Complete one-loop electroweak radiative corrections are calculated in the helicity amplitude approach with allowance for the exact dependence on the muon mass. Numerical results are presented for integrated unpolarized and polarized cross sections as well as angular differential distributions. Calculations are performed using ReneSANCe Monte Carlo generator and MCSANC Monte Carlo integrator.

DOI: 10.1134/S0021364022100460

1. INTRODUCTION

The next generation of electron colliders including the International Linear Collider (ILC) [1–6], the e^+e^- Future Circular Collider (FCCee) [7–11], the Compact Linear Collider (CLIC) [12–14], and the Circular Electron Positron Collider (CEPC) [15] will allow an extensive program of experiments with unique opportunities for precision measurements. A major advantage to fulfill this goal is the universality of linear colliders, as they can operate in four e^+e^-, e^-e^-, $e^-\gamma$, and $\gamma\gamma$ modes with strongly polarized electron and photon beams. An important feature of linear colliders is a high degree of polarization which can be obtained for electron beams.

The Møller scattering along with the Compton-like processes is a good candidate for beam polarization measurements and the background estimation in many searches for new physics beyond the Standard Model. At high energies for the polarized Møller scattering the most advanced Monte-Carlo (MC) tool is needed not only to estimate beam polarization, i.e., polarized experiments CLIC [13], ILC [16], but also to study muon-muon polarized scattering at μ TRISTAN [17].

Equal lepton scattering, $e^-e^- \to e^-e^-$ was first calculated by C. Møller in 1932 [18]. There are a great number of theoretical works for description polarized case of this process [19–26]. In this series of papers, the calculations are given for the QED and electroweak (EW) one-loop corrections with taking into account the polarization.

A calculation of the radiative corrections (RCs) was performed for the unpolarized Møller scattering for the experiment [27] at one-loop level [28, 29], partly at two-loop level [30, 31], and in the first time beyond the ultra-relativistic approximation in [32].

However, all of the above-mentioned studies are not accompanied by the development of the Monte Carlo event generator which is the standard of the modern theoretical support of the high-precision experiments.

The following Monte Carlo generators currently exist, which take into account polarization at tree level: AMEGIC++ [33], based on the helicity amplitudes and being a part of SHERPA; COMPHEP [34], using the traditional trace techniques to evaluate the matrix elements; GRACE [35, 36] (with the packages BASES and SPRING), calculating matrix elements via helicity amplitude techniques; WHIZARD [37] a software system, intended for the effective calculation of scattering cross sections of many-particle and simulated events, where polarization is processed for both the initial and final states.

Theoretical support of experiments by the MERADGEN MC generator for polarized Møller scattering within QED theory is presented in [38].

In our previous works we estimated the theoretical uncertainty for the complete one-loop and leading higher-order EW corrections for e^+e^- and $\gamma\gamma$ polarized

beams. The implementations of polarized Bhabha scattering [39], polarized $e^+e^- \to ZH$ [40], s-channel [41], $e^+e^- \to \gamma Z$ [42] and $\gamma\gamma \to ZZ$ [43] are available in the ReneSANCe MC generator [44] and the MCSANC integrator in the fully massive case and in total phase space.

This article is the next step in the series of SANC papers devoted to the implementation of one of the channels $4f \to 0$, namely, the equal lepton scattering at the one-loop level with allowance for polarization.

The $\alpha(0)$ EW scheme is used in the calculations. All the results are obtained for the center-of-mass (c.m.) energies from $\sqrt{s} = 250$ GeV up to 3 TeV. The sensitivity to the initial polarization for the Born and hard photon bremsstrahlung cross sections was estimated for four beam polarization data sets:

$$\begin{aligned}&(P_{e^-}, P_{e^-})\\ &= (0,0),(-1,-1),(-1,+1),(+1,-1),(+1,+1).\end{aligned} \tag{1}$$

The one-loop contributions were calculated for the following degrees of polarization:

$$(P_{e^-}, P_{e^-}) = (0,0),(\pm 0.8,\pm 0.8). \tag{2}$$

The statistical uncertainties were estimated using the SANC tools: ReneSANCe MC generator and MCSANC integrator.

This article consists of four sections. We describe the methodology of calculations of the polarized cross sections at the complete one-loop EW level within the helicity approach in Section 2. Numerical results and comparison are presented in the Section 3. Summary is drawn in Section 4.

2. ELECTROWEAK ONE-LOOP RADIATIVE CORRECTIONS

We consider the differential cross section for processes

$$\begin{aligned}&l^{\pm}(p_1,\chi_1) + l^{\pm}(p_2,\chi_2)\\ &\to l^{\pm}(p_3,\chi_3) + l^{\pm}(p_4,\chi_4)\ \ (+\gamma(p_5,\chi_5)),\end{aligned} \tag{3}$$

with $l = e,\mu$ and arbitrary longitudinal polarization of initial particles (χ corresponds to the helicity of the particles).

Within the SANC system we calculate all processes using the on-mass-shell renormalization scheme in two gauges: the R_ξ gauge and the unitary gauge as a cross-check.

We apply the helicity approach to all components of the one-loop cross sections:

$$\sigma^{\text{one-loop}} = \sigma^{\text{Born}} + \sigma^{\text{virt}}(\lambda) + \sigma^{\text{soft}}(\lambda,\omega) + \sigma^{\text{hard}}(\omega), \tag{4}$$

where σ^{Born} is the Born cross section, σ^{virt} is the contribution of virtual (loop) corrections, $\sigma^{\text{soft(hard)}}$ is the soft (hard) photon emission contribution (the hard photon energy $E_\gamma > \omega$). The auxiliary parameters λ ("photon mass") and ω are canceled after summation. The corresponding expressions for the Møller scattering cross section cannot be integrated over all angles because the integral diverges.

2.1. Born and Virtual Parts

To calculate the virtual part at the one-loop level using the procedure basement of SANC, we start with considering the covariant amplitude. The covariant one-loop amplitude corresponds to the result of the straightforward standard calculation of all diagrams contributing to a given process at the one-loop level. The covariant amplitude is represented in a certain basis made of strings of Dirac matrices and/or external momenta (structures) contracted with polarization vectors of vector bosons, $\epsilon(k)$, if any.

The covariant amplitude can be written in an explicit form using scalar form factors. All masses, kinematical factors and coupling constant and other parameter dependences are included into these form factors $\mathcal{F}_i$, but tensor structures with Lorenz indices made of strings of Dirac matrices are given by the basis.

The number of form factors is equal to the number of independent structures.

Loop integrals are expressed in terms of standard scalar Passarino–Veltman functions A_0,B_0,C_0,D_0 [45]. We presented the covariant amplitude for the $4f \to 0$ process in [46], where we considered it at the one-loop level of annihilation into a vacuum. Recall that in SANC we always calculate any one-loop process amplitude as annihilation into vacuum with all four-momenta incoming. Therefore, the derived universal scalar form factors for the amplitude of the process $4f \to 0$ after an appropriate permutation of their arguments can be used for the description of the next-to-leading (NLO) corrections of this particular case unfolding into t and u channels.

The virtual (Born) cross section of processes (3) can be written as follows:

$$\frac{d\sigma^{\text{virt(Born)}}_{\chi_1\chi_2}}{d\cos\vartheta_3} = \pi\alpha^2\frac{\beta_s}{2s}\left|\mathcal{H}^{\text{virt(Born)}}_{\chi_1\chi_2}\right|^2, \tag{5}$$

where

$$\left|\mathcal{H}^{\text{virt(Born)}}_{\chi_1\chi_2}\right|^2 = \sum_{\chi_3,\chi_4}\left|\mathcal{H}^{\text{virt(Born)}}_{\chi_1\chi_2\chi_3\chi_4}\right|^2, \tag{6}$$

where m_l is the final lepton mass and $\beta_s = \sqrt{1-\dfrac{4m_l^2}{s}}$, the angle ϑ_3 is the c.m. angle between p_1 and p_3.

Then we estimate the cross section as a function of eight helicity amplitudes. Helicity amplitudes depend

on kinematic variables, coupling constants and seven scalar form factors. Helicity indices $\mathcal{H}_{\chi_1\chi_2\chi_3\chi_4}$ denote the signs of the fermion spin projections to corresponding momenta. Some basic definitions are $c^{\pm} = 1 \pm \cos\vartheta_3$, and the scattering angle ϑ_3 is related to the Mandelstam invariants t,u:

$$t = 2m_l^2 - \frac{s}{2}(1 + \beta_l^2 \cos\vartheta_3), \tag{7}$$

$$u = 2m_l^2 - \frac{s}{2}(1 - \beta_l^2 \cos\vartheta_3). \tag{8}$$

The presence of the electron masses gives additional terms proportional to the factor m_l, which can be considered significant in calculations at low energy.

The set of the corresponding helicity approaches in the t channel for this case is:

$$\mathcal{H}_{\mp\mp\mp\mp} = \frac{1}{t}[(c^+k - 4m_l^2)\tilde{F}_{gg} + \chi_Z(t)((c^+k - 4m_l^2)\tilde{F}_{qq} + 4(k \mp \sqrt{\lambda_e})\tilde{F}_{ll} + 2(c^+k - 4m_l^2 \mp 2\sqrt{\lambda_e})\tilde{F}_{lq} + 2c^- m_l^2 k[\tilde{F}_{qd} + (k \mp \sqrt{\lambda_e})\tilde{F}_{ld}])],$$

$$\mathcal{H}_{\mp--\pm} = \sin\vartheta_3 \frac{\sqrt{s}m_l}{t}[\tilde{F}_{gg} + \chi_Z(t)(\tilde{F}_{qq} + 2\tilde{F}_{lq} - k\tilde{F}_{qd} - (k - \sqrt{\lambda_e})\tilde{F}_{ld})],$$

$$\mathcal{H}_{\pm++\mp} = -\mathcal{H}_{\mp--\pm}(\sqrt{\lambda_e} \to -\sqrt{\lambda_e}),$$

$$\mathcal{H}_{\mp\mp\pm\pm} = -\frac{m_l^2}{t}[2c^+\tilde{F}_{gg} + \chi_Z(t)(2c^+(\tilde{F}_{qq} + 2\tilde{F}_{lq}) + 8\tilde{F}_{ll} - sc^+(\tilde{F}_{ld} + \tilde{F}_{qd}))],$$

$$\mathcal{H}_{\mp\pm\mp\pm} = -\frac{m_l^2}{t}[2c^+\tilde{F}_{gg} + \chi_Z(t)(2c^+(\tilde{F}_{qq} + 2\tilde{F}_{lq}) - sc^+(\tilde{F}_{ld} + \tilde{F}_{qd}))],$$

$$\mathcal{H}_{-\mp\pm-} = -\mathcal{H}_{+\mp\pm+},$$

$$\mathcal{H}_{+\mp\pm+} = \sin\vartheta_3 \frac{\sqrt{s}m_l}{t}[\tilde{F}_{gg} + \chi_Z(t)(\tilde{F}_{qq} + 2\tilde{F}_{lq} - 2m_l^2(\tilde{F}_{ld} + \tilde{F}_{qd}))],$$

$$\mathcal{H}_{\mp\pm\pm\mp} = \frac{c^-}{t}[k\tilde{F}_{gg} + \chi_Z(t)(k(\tilde{F}_{qq} + 2\tilde{F}_{lq}) - 2m_l^2[(k \pm \sqrt{\lambda_e})\tilde{F}_{ld} + k\tilde{F}_{qd}])].$$

Here $\chi_Z(t)$ is the Z/γ propagator ratio:

$$\chi_Z(t) = \frac{1}{4s_W^2 c_W^2}\frac{t}{t - M_z^2}. \tag{9}$$

Note that *tilted* form factors absorb couplings, which leads to a compactification of formulas for the amplitude, while explicit expressions will be given for *untilted* quantities.

The expressions for *tiled* form factors are:

$$\tilde{F}_{gg} = (I_l^{(3)})^2 F_{gg}(s,t,u), \tag{10}$$

$$\tilde{F}_{ll} = \delta_l^2 F_{ll}(s,t,u),$$

$$\tilde{F}_{qq} = I_l^{(3)}\delta_l F_{qq}(s,t,u),$$

$$\tilde{F}_{lq} = \delta_l I_l^{(3)} F_{lq}(s,t,u),$$

$$\tilde{F}_{ql} = \delta_l I_l^{(3)} F_{ql}(s,t,u),$$

$$\tilde{F}_{ld} = (I_l^{(3)})^2 F_{ld}(s,t,u),$$

$$\tilde{F}_{qd} = \delta_l I_l^{(3)} F_{qd}(s,t,u).$$

We also use the coupling constants

$$I_l^{(3)}, \quad \sigma_l = v_l + a_l, \quad \delta_l = v_l - a_l,$$

$$s_W = \frac{e}{g}, \quad c_W = \frac{M_W}{M_Z},$$

with $l = e,\mu$.

In order to get helicity approaches for the Born level, one should set $F_{gg,ll,lq,ql,qq} = 1$ and $F_{ld,qd} = 0$.

2.2. Real Photon Emission Corrections

The real corrections consist of soft and hard radiative contributions. They are calculated using the bremsstrahlung modules. The soft bremsstrahlung has a Born-like kinematics, while the phase space of hard radiation has an extra particle, a photon.

The *soft bremsstrahlung* has the form

$$\sigma^{\text{soft}} = -Q_e^2 \frac{2\alpha}{\pi}\sigma^{\text{Born}}\left[(1 + \frac{1 - 2m_l^2/s}{\beta_s}\ln x^2)\ln\left(\frac{4\omega^2}{\lambda^2}\right) + \frac{1}{\beta_s}\left[-\ln x^2 + (1 - 2m_l^2/s)(\text{Li}_2(1 - x^2) - \text{Li}_2\left(1 - \frac{1}{x^2}\right))\right] - F(t) - F(u)\right], \tag{11}$$

where

$$F(I) = \frac{1 - 2m_l^2/I}{\beta_I}\left[\ln y_I \ln\left(\frac{4\omega^2}{\lambda^2}\right) + \text{Li}_2\left(1 - \frac{y_I x}{z_I}\right) - \text{Li}_2\left(1 - \frac{x}{z_I}\right) + \text{Li}_2\left(1 - \frac{y_I}{z_I x}\right) - \text{Li}_2\left(1 - \frac{1}{z_I x}\right)\right],$$

$$\beta_I = \sqrt{1 - \frac{4m_l^2}{I}}, \quad x = \frac{\sqrt{s}}{m_l}\frac{1 + \beta_s}{2},$$

$$y_I = 1 - \frac{I}{m_l^2}\frac{1 + \beta_I}{2}, \quad z_I = \frac{m_l}{\sqrt{s}}(1 + y_I),$$

Table 1. Tuned triple comparison between SANC (the second column), WHIZARD (the third column), and CalcHEP (the fourth column) and SANC results for the hard bremsstrahlung cross section

P_{e^-}, P_{e^-}	S	W	C
0, 0	170.12(1)	170.13(1)	170.11(2)
−1, −1	284.58(1)	284.58(1)	284.55(2)
−1, 1	74.00(1)	74.00(1)	74.00(2)
1, −1	74.01(1)	74.02(1)	74.00(2)
1, 1	247.90(1)	247.90(1)	247.86(2)

with $I = t,u$.

In presenting the results we used our universal massive module for the *hard photon bremsstrahlung* for $4f\gamma \to 0$ [41] by appropriate unfolding it in the right channel.

3. NUMERICAL RESULTS

3.1. Tree Level

In this section calculated polarized cross sections at tree level for the Born and hard photon bremsstrahlung are compared with the results of the CalcHEP [34] and WHIZARD [37, 47, 48] codes.

The results are calculated in the $\alpha(0)$ EW scheme with fixed 100% polarized initial states for $\sqrt{s}$ = 250 GeV and angular cuts $|\cos\vartheta_e| \le 0.9$. For the hard bremsstrahlung cross sections, an additional cut on the photon energy $E_\gamma \ge \omega = 10^{-4}\sqrt{s}/2$ is applied.

The Born results agree in all digits for all codes, and therefore the table is omitted. The hard bremsstrahlung results are shown in Table 1. Very good agreement within statistical errors with the above-mentioned codes is found.

3.2. One-Loop Level

In this Section we show the study of the complete one-loop EW RCs and polarization effects for Møller scattering in high-energy regions. Numerical estimates are presented for the total (integrated) cross sections (σ, pb) and relative corrections (δ, %) as well as for the differential distribution as function of the scattering angle $\cos\vartheta_3$. The channels e^- ($e^-e^- \to e^-e^-(\gamma)$) and μ^+ ($\mu^+\mu^+ \to \mu^+\mu^+(\gamma)$) of reaction (3) are considered below.

3.2.1. Integrated cross sections. CLIC would provide high-luminosity e^-e^- collisions covering a center-of-mass energy range from 0.38 to 3 TeV. They are three main c.m. energy stages at $\sqrt{s}_{\rm CLIC}$: 0.38, 1.5, and 3 TeV.

Table 2. Integrated Born and one-loop cross section in pb and relative corrections in percent for e^--channel scattering for c.m. energy $\sqrt{s}_{\rm ILC\&CLIC}$ and set (2) of the initial particle polarization degrees in the $\alpha(0)$ EW scheme

P_{e^-}, P_{e^-}	0, 0	0.8, 0.8	−0.8, −0.8
$\sqrt{s}$ = 250 GeV			
$\sigma^{\rm Born}$, pb	94.661(1)	120.152(1)	136.377(1)
$\sigma^{\rm one\text{-}loop}$, pb	103.906(2)	134.976(2)	147.224(2)
δ, %	9.77(1)	12.34(1)	7.95(1)
$\sqrt{s}$ = 380 GeV			
$\sigma^{\rm Born}$, pb	42.969(1)	55.739(1)	65.487(1)
$\sigma^{\rm one\text{-}loop}$, pb	47.327(1)	63.264(1)	70.345(1)
δ, %	10.14(1)	13.50(1)	7.42(1)
$\sqrt{s}$ = 500 GeV			
$\sigma^{\rm Born}$, pb	25.498(1)	33.430(1)	39.984(1)
$\sigma^{\rm one\text{-}loop}$, pb	28.068(1)	38.171(2)	42.627(2)
δ, %	10.08(1)	14.18(1)	6.61(1)
$\sqrt{s}$ = 1 TeV			
$\sigma^{\rm Born}$, pb	6.657(1)	8.850(1)	10.865(1)
$\sigma^{\rm one\text{-}loop}$, pb	7.218(1)	10.229(1)	11.104(1)
δ, %	8.42(1)	15.58(1)	2.20(1)
$\sqrt{s}$ = 1.5 TeV			
$\sigma^{\rm Born}$, pb	2.992(1)	3.989(1)	4.928(1)
$\sigma^{\rm one\text{-}loop}$, pb	3.185(1)	4.635(1)	4.827(1)
δ, %	6.46(1)	16.19(1)	−2.06(1)
$\sqrt{s}$ = 3 TeV			
$\sigma^{\rm Born}$, pb	0.7536(1)	1.007(1)	1.249(1)
$\sigma^{\rm one\text{-}loop}$, pb	0.7665(1)	1.177(1)	1.103(1)
δ, %	1.71(1)	16.94(1)	−11.70(1)

The ILC offers many opportunities for measurements with collider energies from 90 GeV to 1 TeV. Three main c.m. energy stages can be distinguished: $\sqrt{s}_{\rm ILC}$ = 0.25, 0.5, and 1 TeV, with electron polarization of $P_{e^-} = \pm 0.8$.

Table 2 presents the integrated Born and one-loop cross section in pb and relative corrections in percent for the e^--channel for c.m. energy $\sqrt{s}_{\rm ILC\&CLIC}$ and set (2) of the initial particle polarization degrees in the $\alpha(0)$ EW scheme.

Under the μTRISTAN experimental conditions, the energy is assumed to be $\sqrt{s}_{\mu\rm TRISTAN}$: 0.6, 1, 2 TeV

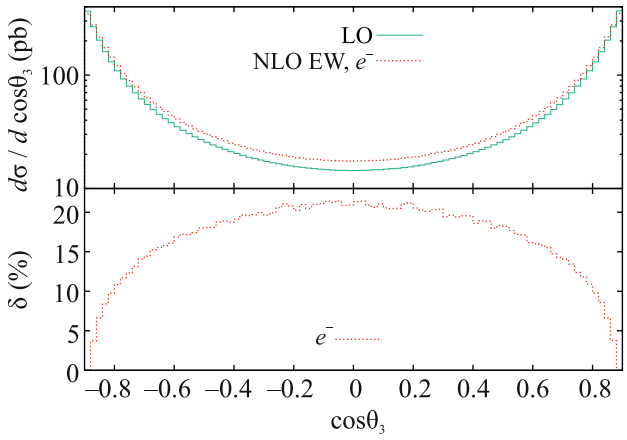

Fig. 1. (Color online) LO and NLO EW unpolarized cross sections (upper panel) and relative corrections (lower panel) of the e^--channel for the c.m. energy $\sqrt{s} = 250$ GeV versus $\cos\theta_3$.

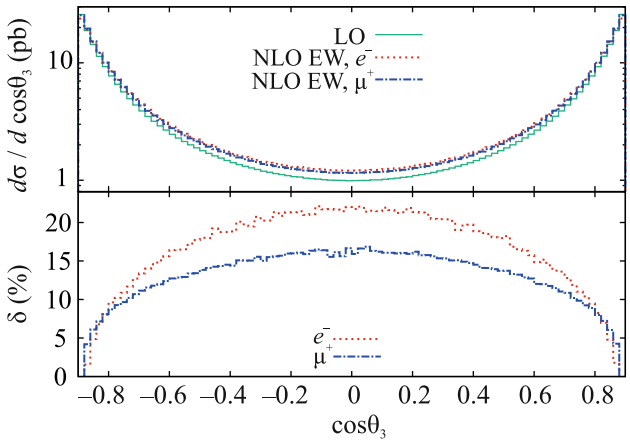

Fig. 2. (Color online) LO and NLO EW unpolarized cross sections (upper panel) and relative corrections (lower panel) of the e^-- and μ^+-channels for the c.m. energy $\sqrt{s} = 1000$ GeV versus $\cos\theta_3$.

and the polarization of both beams will reach $P_{\mu^+} = \pm 0.8$ for the μ^+-channel. Table 3 presents the same observables as in Table 2 in the conditions of the μTRISTAN experiment.

As it seen in Tables 2 and 3, the use of the polarized beams significantly increases the cross section. At the same time the RCs increase at $P_{e^-} = (0.8, 0.8)$ and reduce at $P_{e^+} = (-0.8, -0.8)$ comparing to the unpolarized case in the region of c.m. energies $\sqrt{s} = 250$–1000 GeV. At higher c.m. energies the polarization $P_{e,\mu} = (\pm 0.8, \pm 0.8)$ increases the cross section as well, but the absolute value of the relative correction became larger than for the unpolarized one.

Table 3. Integrated Born and one-loop cross section in pb and relative corrections in percent for the μ^+-channel for c.m. energy $\sqrt{s}_{\mu\text{TRISTAN}}$ and set (2) of the initial particle polarization degrees in the $\alpha(0)$ EW scheme

P_{μ^+}, P_{μ^+}	0, 0	0.8, 0.8	–0.8, –0.8
$\sqrt{s} = 600$ GeV			
σ^{Born}, pb	17.974(1)	23.690(1)	28.601(1)
$\sigma^{\text{one-loop}}$, pb	19.715(1)	27.064(1)	30.160(1)
δ, %	9.69(1)	14.24(1)	5.45(1)
$\sqrt{s} = 1$ TeV			
σ^{Born}, pb	6.6572(1)	8.8497(1)	10.8648(1)
$\sigma^{\text{one-loop}}$, pb	7.2019(1)	10.1930(1)	11.0589(2)
δ, %	8.18(1)	15.18(1)	1.79(1)
$\sqrt{s} = 2$ TeV			
σ^{Born}, pb	1.6903(1)	2.2559(1)	2.7935(1)
$\sigma^{\text{one-loop}}$, pb	1.7646(1)	2.6195(1)	2.6210(1)
δ, %	4.40(1)	16.12(1)	–6.17(1)

3.2.2. Differential cross sections. Figures 1 and 2 show the differential distributions for the LO and EW NLO cross sections (in pb) as well as the relative corrections (in %) for the e^-- and μ^+-channels for the c.m. energies $\sqrt{s} = 250$, 1000 GeV as a function of $\cos\theta_3$.

The differential distributions over $\cos\theta_3$ are symmetric for all c.m. energies and the maximum of the relative corrections is at the zero angle while the minimum is close to the $|\cos\theta_3| = 1$. This is due to dominance of the Born contribution in the $|\cos\theta_3| \approx 1$ region due to a photon propagator $1/t$ $(1/u)$.

It should be noted that while the integrated relative corrections for the c.m. energy $\sqrt{s} = 1000$ GeV for the e^-- and μ^+-channels differ by 0.4% (see Tables 2, 3) the differential difference is larger, being about 5–6% at $\cos\theta_3 = 0$.

4. SUMMARY

We computed the NLO contributions RCs due to QED and purely weak corrections and implement them into a fully differential Monte Carlo event generator ReneSANCe and MCSANC integrator.

We presented explicit expressions for helicity approaches to evaluate virtual and soft parts for Møller scattering. We used our previous module for helicity

approaches of the hard photon bremsstrahlung [41]. We showed the results of interest for unpolarized FCCee and polarized ILC, CLIC, μTRISTAN experiments.

Since the measurement of the beam polarization is expected at the level of 1% [19, 49], it is necessary to include more than one-loop EW RCs (leading logarithms QED and EW 2-loop corrections) to ensure the required level of the theoretical support.

The established SANC framework allows us to investigate the one-loop and higher-order corrections for any polarization, estimate the contribution of the selected helicity state, and take into account mass effects.

ACKNOWLEDGMENTS

We are grateful to M. Potapov for the help in preparation of the manuscript.

FUNDING

This work was supported by the Russian Foundation for Basic Research, project no. 20-02-00441.

CONFLICT OF INTEREST

The authors declare that they have no conflicts of interest.

OPEN ACCESS

REFERENCES

1. ILC. https://www.linearcollider.org/ILC.
2. A. Irles, R. Poschl, F. Richard, and H. Yamamoto, in *Proceedings of the Linear Collider Community Meeting, Lausanne, Switzerland, April 8–9, 2019* (2019), arXiv: 1905.00220.
3. G. Moortgat-Pick, H. Baer, M. Battaglia, et al., Eur. Phys. J. C **75**, 371 (2015); arXiv: 1504.01726.
4. H. Baer, T. Barklow, K. Fujii, et al., arXiv: 1306.6352.
5. E. Accomando, A. Andreazza, H. Anlauf, et al. (ECFA/DESY LC Physics Working Group Collab.), Phys. Rep. **299**, 1 (1998); hep-ph/9705442.
6. E. Accomando, A. Aranda, E. Ateser, et al. (CLIC Physics Working Group Collab.), in *Proceedings of the 11th International Conference on Hadron Spectroscopy (Hadron 2005), Rio de Janeiro, Brazil, August 21–26, 2005* (2004), hep-ph/0412251.
7. FCC-ee. http://tlep.web.cern.ch.
8. FCC Collab., A. Abada, M. Abbrescia, S. S. Abdus Salam, et al., Eur. Phys. J. ST **228**, 1109 (2019).
9. FCC Collab., A. Abada, M. Abbrescia, S. S. Abdus Salam, et al., Eur. Phys. J. C **79**, 474 (2019).
10. A. Blondel and P. Janot, arXiv: 1912.11871.
11. A. Blondel, J. Gluza, S. Jadach, et al., in *Proceedings of the Mini Workshop on Precision EW and QCD Calculations for the FCC Studies: Methods and Techniques, CERN, Geneva, Switzerland, January 12–13, 2018* (CERN, Geneva, 2019), Vol. 3; arXiv: 1809.01830.
12. CLIC. http://clic-study.web.cern.ch.
13. M. J. Boland, U. Felzmann, P. J. Giansiracusa, et al. (CLIC, CLICdp Collab.), arXiv: 1608.07537.
14. T. K. Charles, P. J. Giansiracusa, T. G. Lucas, et al. (CLICdp, CLIC Collab.), CERN Yellow Rep. Monogr. **1802**, 1 (2018); arXiv: 1812.06018.
15. CEPC. http://cepc.ihep.ac.cn.
16. K. Fujii, C. Grojean, M. E. Peskin, et al., arXiv: 2007.03650.
17. Y. Hamada, R. Kitano, R. Matsudo, H. Takaura, and M. Yoshida, arXiv: 2201.06664.
18. C. Møller, Ann. Phys. **14**, 531 (1932).
19. S. Jadach and B. F. L. Ward, Phys. Rev. D **54**, 743 (1996).
20. N. M. Shumeiko and J. G. Suarez, J. Phys. G **26**, 113 (2000); hep-ph/9912228.
21. J. C. Montero, V. Pleitez, and M. C. Rodriguez, Phys. Rev. D **58**, 094026 (1998); hep-ph/9802313.
22. A. Denner and S. Pozzorini, Eur. Phys. J. C **7**, 185 (1999); hep-ph/9807446.
23. A. Czarnecki and W. J. Marciano, Int. J. Mod. Phys. A **15**, 2365 (2000); hep-ph/0003049.
24. G. Alexander and I. Cohen, Nucl. Instrum. Methods Phys. Res., Sect. A **486**, 552 (2002); hep-ex/0006007.
25. F. J. Petriello, Phys. Rev. D **67**, 033006 (2003); hep-ph/0210259.
26. A. Ilyichev and V. Zykunov, Phys. Rev. D **72**, 033018 (2005); hep-ph/0504191.
27. J. Benesch, P. Brindza, R. D. Carlini, et al. (MOLLER Collab.), arXiv: 1411.4088.
28. A. Aleksejevs, S. Barkanova, A. Ilyichev, and V. Zykunov, Phys. Rev. D **82**, 093013 (2010); arXiv: 1008.3355.
29. A. I. Ahmadov, Y. M. Bystritskiy, E. A. Kuraev, A. N. Ilyichev, and V. A. Zykunov, Eur. Phys. J. C **72**, 1977 (2012); arXiv: 1201.0460.
30. A. G. Aleksejevs, S. G. Barkanova, Y. M. Bystritskiy, E. A. Kuraev, and V. A. Zykunov, Phys. Part. Nucl. Lett. **13**, 310 (2016); arXiv: 1508.07853.
31. J. Erler, R. Ferro-Hernández, and A. Freitas, arXiv: 2202.11976.
32. I. Akushevich, H. Gao, A. Ilyichev, and M. Meziane, Eur. Phys. J. A **51** (1), 1 (2015).
33. F. Krauss, R. Kuhn, and G. Soff, J. High Energy Phys., No. 02, 044 (2002); hep-ph/0109036.

34. A. Belyaev, N. D. Christensen, and A. Pukhov, Comput. Phys. Commun. **184**, 1729 (2013); arXiv: 1207.6082.
35. J. Yuasa, J. Fujimoto, T. Ishikawa, M. Jimbo, T. Kaneko, K. Kato, S. Kawabata, T. Kon, Y. Kurihara, M. Kuroda, N. Nakazawa, Y. Shimizu, and H. Tanaka, Prog. Theor. Phys. Suppl. **138**, 18 (2000); hep-ph/0007053.
36. G. Belanger, F. Boudjema, J. Fujimoto, T. Ishikawa, T. Kaneko, K. Kato, and Y. Shimizu, Phys. Rep. **430**, 117 (2006); hep-ph/0308080
37. W. Kilian, T. Ohl, and J. Reuter, Eur. Phys. J. C **71**, 1742 (2011); arXiv: 0708.4233.
38. A. Afanasev, E. Chudakov, A. Ilyichev, and V. Zykunov, Comput. Phys. Commun. **176**, 218 (2007); hep-ph/0603027.
39. D. Bardin, Y. Dydyshka, L. Kalinovskaya, L. Rumyantsev, A. Arbuzov, R. Sadykov, and S. Bondarenko, Phys. Rev. D **98**, 013001 (2018); arXiv: 1801.00125.
40. S. Bondarenko, Y. Dydyshka, L. Kalinovskaya, L. Rumyantsev, R. Sadykov, and V. Yermolchyk, Phys. Rev. D **100**, 073002 (2019); arXiv: 1812.10965.
41. S. Bondarenko, Y. Dydyshka, L. Kalinovskaya, R. Sadykov, and V. Yermolchyk, Phys. Rev. D **102**, 033004 (2020); arXiv: 2005.04748.
42. S. Bondarenko, Y. Dydyshka, L. Kalinovskaya, L. Rumyantsev, R. Sadykov, and V. Yermolchyk, arXiv: 2111.11490.
43. S. Bondarenko, L. Kalinovskaya, and A. Sapronov, arXiv: 2201.04350.
44. R. Sadykov and V. Yermolchyk, Comput. Phys. Commun. **256**, 107445 (2020); arXiv: 2001.10755.
45. G. Passarino and M. J. G. Veltman, Nucl. Phys. B **160**, 151 (1979).
46. A. Andonov, D. Bardin, S. Bondarenko, P. Christova, L. Kalinovskaya, and G. Nanava, Phys. Part. Nucl. **34**, 577 (2003); hep-ph/0207156.
47. T. Ohl, in *Proceedings of the LoopFest V: Radiative Corrections for the International Linear Collider: Multiloops and Multilegs, SLAC, Menlo Park, CA, June 19–21, 2006* (2006).
48. W. Kilian, S. Brass, T. Ohl, J. Reuter, V. Rothe, P. Stienemeier, and M. Utsch, in *Proceedings of the International Workshop on Future Linear Collider LCWS'2017 Strasbourg, France, October 23–27, 2017* (2018); arXiv: 1801.08034.
49. T. Abe, N. Arkani-Hamed, D. Asner, et al., hep-ex/0106058.